Journal of Modern Computing and Engineering Research
JMCER
Volume 2025,p. 42-52
https://jmcer.org

Design and Simulation of a Quad-Transmission-Zero Microwave Bandpass Filter

Thaer A. Sultan[1], Ahmed M A Sabaawi[2*],
[1,2]*College of Electronics Engineering, University of Nineveh, Electronic Engineering Department, Nineveh, Iraq*
[1]*thaer.ahmed.eng22@stu.uoninevah.edu.iq*, [2*] *ahmed.sabaawi@uoninevah.edu.iq*

Received: March 27, 2025 Revised: June 18,2025 Accepted: June 23, 2025

Abstract:
This paper details the design and simulation of a compact microstrip bandpass filter that incorporates four transmission zeros, aiming to significantly enhance its selectivity and stopband performance for diverse modern wireless applications, including 5G networks, radar systems, and satellite communication, by establishing a clear methodology for integrating these zeros into a compact design while maintaining optimal bandwidth and insertion loss. The filter, cantered at 3.5 GHz with a 0.6 GHz bandwidth, employs folded resonators (FRs) for bandwidth control and coupling resonators (CRs) for transmission zero (TZ) generation. Input/output coupling and a zero-degree feed technique are implemented to introduce four TZs, significantly improving stopband performance. Optimization of resonator spacing and feed line positions ensures minimized insertion loss (-1.147 dB) and high return loss (> -40 dB). The proposed microstrip filter, with dimensions of 0.39 $\lambda g \times 0.46$ λg, has been simulated by software ADS using an FR-4 substrate with a thickness of 1.6 mm and a dielectric constant (εr) of 4.3, demonstrating superior performance compared to existing designs, featuring a compact size and enhanced stopband attenuation through the strategic placement of TZs.

Keywords: *Microstrip Bandpass Filter, 5G, Compact BPF, Advanced Design System.*

1 Introduction

In the rapidly evolving landscape of wireless communication, encompassing cutting-edge fifth-generation (5G) systems, Wireless Local Area Networks (WLANs), Worldwide Interoperability for Microwave Access (WiMAX), radar, and satellite communication, bandpass filters (BPFs) are not merely components but foundational elements. Their significance intensifies as technological advancements push towards utilizing a broader spectrum of frequencies, from the mid-band (sub-6 GHz) to the high-band (millimeter wave). The core function of these filters lies in their ability to precisely manage signal flow: they meticulously permit the passage of desired frequencies while effectively attenuating undesirable ones. This critical role in optimizing circuit performance drives a substantial demand for BPFs characterized by high performance metrics, planar configurations, and compact dimensions (Costanzo and Masotti, 2017, Ezhilarasan and Dinakaran, 2017, Thompson et al., 2014, Christiano and Fitzgerald, 2003).

Extensive research has been dedicated to developing BPFs with simplified structures, minimized form factors, planar topologies, low insertion loss, and high return loss. This pursuit has led to the exploration of a diverse array of design methodologies and architectural approaches. Early designs, for instance, as demonstrated by (Astuti and Alaydrus (2013) and Maulidini et al. (2020)), often employed square open-loop resonators and fundamental coupling schemes to achieve necessary selectivity. Later, (Chang et al. (2019) and Kadiri et al. (2022)) advanced these efforts by introducing internal coupling to improve stopband suppression. A particularly promising avenue for enhancing filter performance has been the strategic application of cross-coupling techniques. This method, which involves creating multiple signal pathways, has proven highly effective in various designs. For example, a filter incorporating six resonators with strategic cross-coupling showcased superior selectivity and stopband rejection (Astuti and Alaydrus, 2013). Similarly, designs utilizing four resonators, also leveraging cross-coupling, yielded favorable response characteristics (Alaydrus et al.,

Corresponding author: Author name and email

2013; Chang et al., 2019; Kadiri et al., 2022; Maulidini et al., 2020). These studies collectively underscore the efficacy of cross-coupling in realizing high-performance BPFs, striking a crucial balance between robust performance and manageable design complexity. However, a recurring limitation in many of these designs has been their inability to achieve sharp transition slopes and sufficient stopband attenuation while maintaining a compact footprint. Critically, most existing filters typically introduce only one or two TZs. This constraint severely limits their effectiveness in suppressing out-of-band signals and often lacks the flexibility for independent control over multiple TZs, or the ability to maintain compact size alongside wide bandwidth. Furthermore, these works often do not fully exploit the potential of zero-degree feed structures, and recent designs frequently lack the flexibility to adjust TZ locations independently, thereby restricting their applicability in dynamically reconfigurable systems.

This research addresses these existing challenges by proposing an advanced BPF design that strategically integrates four controllable transmission zeros through the innovative combination of folded microstrip resonators and zero-degree feed techniques. This novel approach builds upon previous efforts, but critically overcomes their limitations by combining folded resonators with both coupling and zero-degree feed mechanisms. This allows for the generation of multiple controllable TZs while simultaneously ensuring compactness and low insertion loss, thereby filling significant gaps in adaptability and stopband control. The detailed design process begins with establishing fundamental characteristics through the folded microstrip resonators, enabling precise calibration of the center frequency and bandwidth. Subsequently, coupling resonators are meticulously engineered to introduce transmission zeros within the stopband, utilizing both input/output coupling (Shen et al., 2019) and zero-degree feed (Tsai et al., 2002) techniques. The methodology further refines bandwidth optimization by adjusting the coupling between folded resonators and meticulously shaping resonators to facilitate enhanced coupling and performance. Precise control over transmission zero placement is achieved through the careful manipulation of coupling distances, and optimal resonator coupling is realized via iterative adjustments. To significantly augment stopband attenuation, a zero-degree feed approach is implemented, introducing additional transmission zeros by strategically injecting signals, with fine-tuned feed point adjustments further refining the overall performance. This systematic approach is meticulously designed to yield a compact, high-performance filter characterized by a clearly defined passband and strategically positioned transmission zeros for superior attenuation. The proposed BPF's performance has been rigorously simulated using Advanced Design System (ADS) software, employing an FR4 substrate with a relative permittivity of 4.3, a thickness of 1.6 mm, and a tangent loss of 0.01. This design holds substantial promise for seamless future integration into next-generation 5G infrastructure, advanced radar systems, and cutting-edge satellite communication units. Its intrinsic compact footprint and significantly improved selectivity make it suited for the densely packed communication modules prevalent in modern systems. Furthermore, the inherent modularity of this design allows for remarkable scalability and adaptability to future frequency bands or emerging wireless standards through only minor geometric modifications, ensuring its relevance in an ever-evolving technological landscape.

2 Filter’s Design

For the design of the proposed filter, a pair of FRs are initially developed. These resonators are chosen due to their ability to reduce overall circuit size without affecting the resonant frequency, as demonstrated in previous miniaturized BPF designs. The center frequency is determined by calibrating the total electrical length of the FRs, while the bandwidth is defined by controlling the electromagnetic coupling between them. The coupling strength, and thus the bandwidth, is fine-tuned by adjusting the gap between the resonators. Subsequently, another pair of CRs will be designed to generate two pairs of transmission zeros within the stopband region surrounding the passband. This will be achieved using two methods: first, input/output coupling, and second, zero-degree feed.

2.1 Bandwidth Optimization Through Folded Resonators (FRs) Coupling

The initial phase of the design procedure involves the creation of a uniform impedance resonator (UIR), whose length is calibrated to be half of the signal's wavelength at the filter's central frequency, a methodology extensively documented in reference

(Hong and Lancaster, 2004). To reduce the overall size, the UIR undergoes a series of symmetrical folds, a process that does not alter the original resonance frequency. The resulting folded resonator (FR), along with its frequency response under conditions of weak coupling, is depicted in Figure (1).

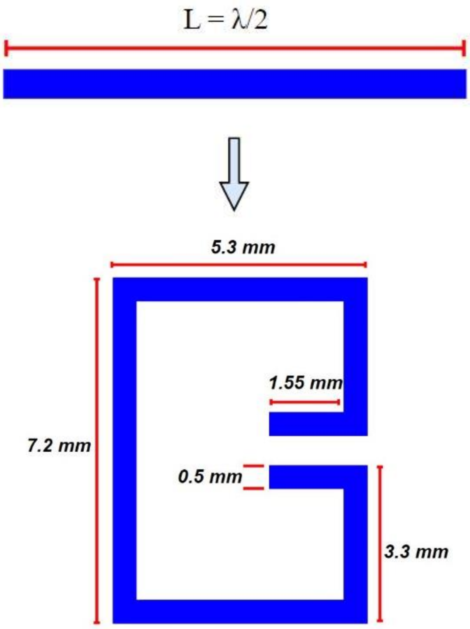

(a)

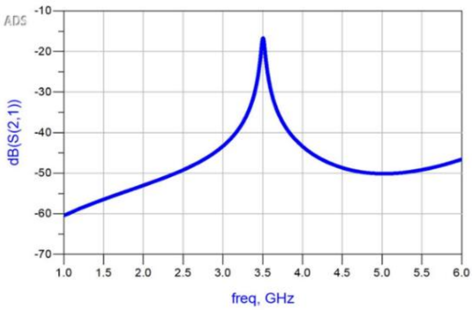

(b)

Figure 1: (a) FR's Geometry; (b) Frequency Response of the FR.

Following this, two identical FRs are positioned in a mirrored, back-to-back arrangement, separated by a gap (s), as shown in Figure (2a). Introducing a low-level voltage to the neighbouring FRs initiates coupling, leading to the formation of two separate frequencies, f1 and f2, as illustrated in Figure (2b). These frequencies establish the boundaries of the passband, with the bandwidth being directly determined by their difference.

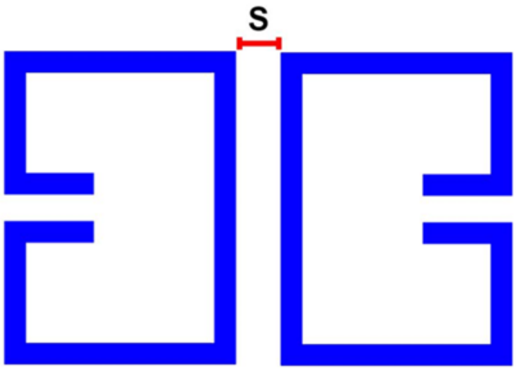

(a)

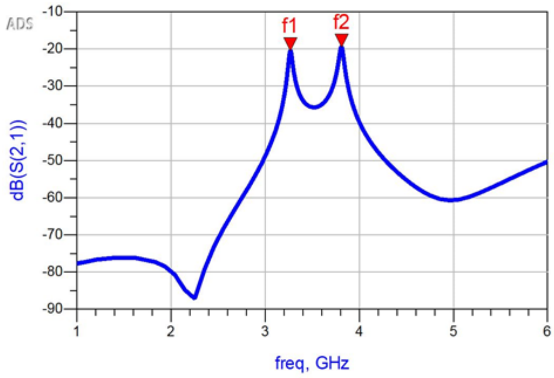

(b)

Figure 2: (a) FRs Structure separated by (s); (b) Frequency Response of the Coupled FRs.

The precise adjustment of the bandwidth is achieved by modifying the coupling intensity: a reduction in (s), indicating stronger coupling, results in a wider bandwidth, while an increase in (s), signifying weaker coupling, leads to a narrower bandwidth. Figure (3) illustrates the influence of varying (s) on f1 and f2.

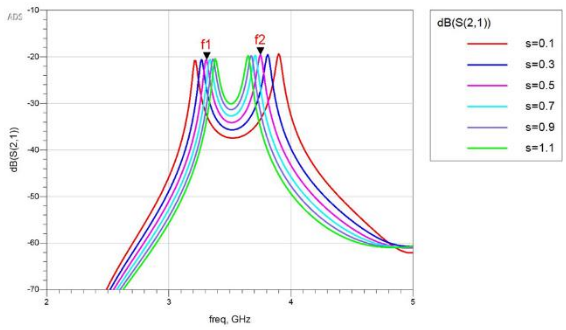

Figure 3: Effect of distance (s) on frequencies (f1 and f2).

The coupling intensity between the FRs bears an inverse relationship to (s). A diminished (s) facilitates the transmission of frequencies closer to the center frequency, thereby expanding the bandwidth. Conversely, an elevated (s) restricts the bandwidth. In this particular design, a separation of (s = 0.5 mm) was chosen to yield an approximate bandwidth of 0.6 GHz.

2.2 A pair of TZs Generation and Feed Lines Design

Subsequent to the development of the FRs and the establishment of the desired bandwidth, CRs are engineered. These CRs function as feed lines for the FRs and facilitate source-load coupling, consequently producing a pair of TZs surrounding the passband. This outcome is realized by establishing two discrete signal pathways: one that traverses the FRs and another that directly connects the CRs, as visually represented in Figure (4).

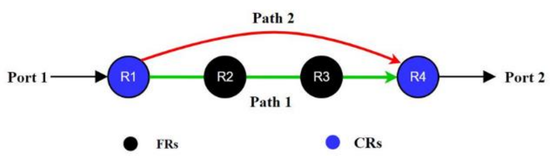

Figure 4: Dual Signal Paths for TZs Generation.

The inception of the CR design is rooted in a Uniform Impedance Resonator (UIR) (Figure (5a)), whose length is equivalent to half the signal's wavelength at the filter's central frequency. This UIR is then transformed into a near-square configuration (Figure (5b)), a shape that is advantageous for encapsulating the FRs, attaining optimal coupling, and ensuring appropriate feeding. This configuration also streamlines source-load coupling, owing to the close spatial relationship between the CR extremities. Further improvements in source-load coupling are achieved by introducing right-angle folds at both ends of the CRs (Figure (5c)). The CRs are then supplied with input signals through feed lines at precisely calculated locations, determined using equation (1) as outlined in (Surwase et al., 2017), as shown in Figure (5d)

$$t = \frac{2L}{\pi} sin^{-1}\left(\sqrt{\frac{\pi}{2}\frac{Z_0/Z_r}{Q_e}}\right) \tag{1}$$

Where 't' represents the distance from the resonator's midpoint to the injection point, 'L' denotes the resonator's length, 'Zr' signifies the resonator's impedance, 'Z0' represents the source impedance, and 'Qe' designates the external quality factor.

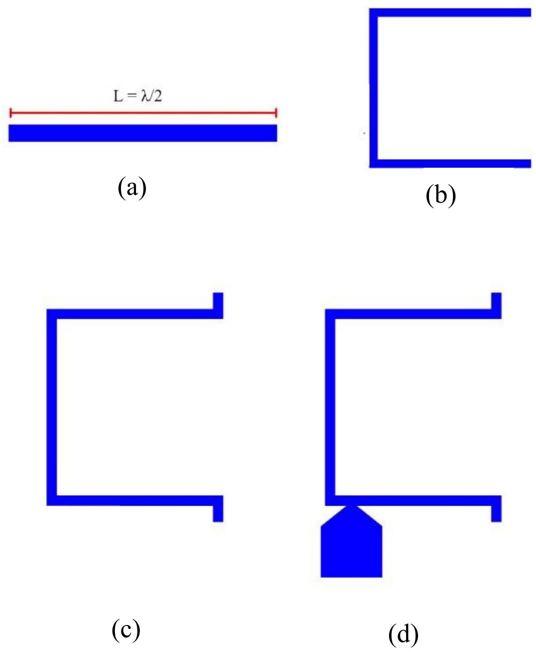

Figure 5: Coupling Resonator (CR) Evaluation.

After finalizing the design of the filter's constituent elements, the next critical phase involves the creation and precise positioning of the two transmission zeros at the passband's boundaries, as previously elaborated. This objective is met by inducing

JMCER

coupling between the two CRs and establishing two distinct signal pathways, specifically through the manipulation of the separation distance (d) between them, as depicted in Figure (6a). This spatial adjustment directly regulates the coupling intensity between the resonators, thereby generating and influencing the placement of the TZ surrounding the passband. Figure (6b) showcases the filter's frequency response across a range of (d) values.

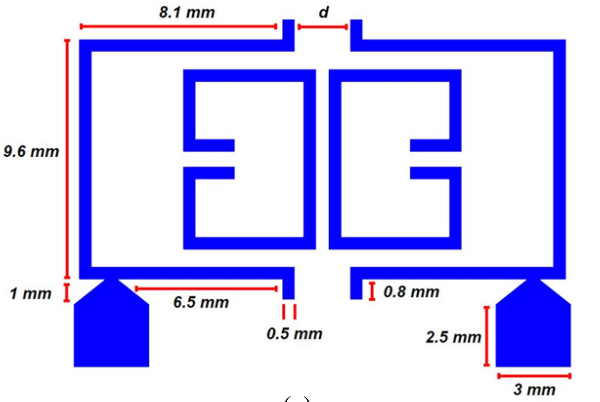

(a)

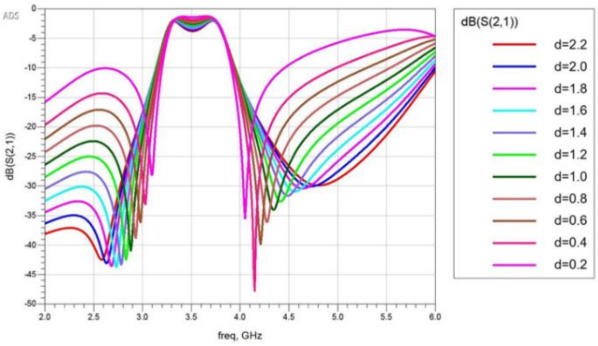

(b)

Figure 6: (a) Creating two paths for the signal by CRs coupling; (b) Effect of strengthen Coupling between CRs on generating a pair of TZs.

Figure (6) visually presents the progression of the TZs around the passband. Reducing the separation (d) augments the coupling strength, consequently intensifying the impact of the TZs and causing them to converge towards the passband. A separation of (d = 0.4 mm) was chosen, as this configuration yields a pair of TZs located approximately at fz1 = 3 GHz and fz2 = 4.3 GHz.

2.3 Optimal coupling between FRs and CRs

With a clear understanding of how the coupling between the CRs directly influences the creation and positioning of the TZs, the focus shifts to examining the impact of the coupling intensity between the CRs and the FRs on the filter's frequency response. This is accomplished by systematically decreasing the separation between them from all directions until an optimal coupling arrangement is identified, resulting in the most favorable filter performance. Initially, the spacing between the CRs and FRs is symmetrically modified from the upper and lower regions by altering the distance (d), as illustrated in Figure (7a). Concurrently, the lengths X and Y of the CRs are adjusted to maintain their resonant frequency at a stable value.

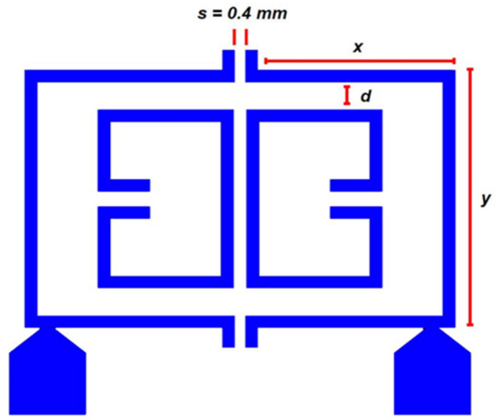

(a)

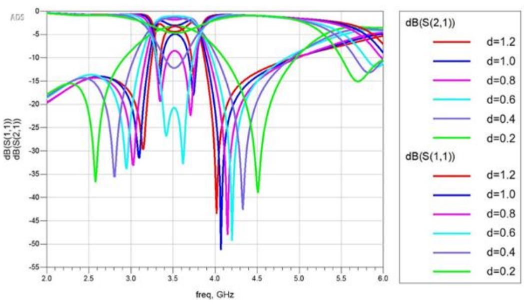

(b)

Figure 7: (a) Adjustment of top and bottom coupling strength between FRs and CRs; (b) Effect of strengthen Coupling between FRs and CRs on the filter response.

Figure (7b) demonstrates the fluctuations in the filter's frequency response as (d) is varied. It is noted that a separation of approximately (6 mm) between the CRs and FRs, measured from both the top and bottom, produces the most desirable filter response for this specific configuration.

Having determined the optimal vertical spacing between the CRs and FRs, the subsequent phase involves folding both CRs inward from their midpoint, as shown in Figure 8. This alteration serves a dual purpose: it reduces the overall dimensions of the filter, rendering it more compact, particularly after the preceding adjustments, and it expands the coupling surface area, facilitating smoother wave transmission through the filter and enhancing overall performance.

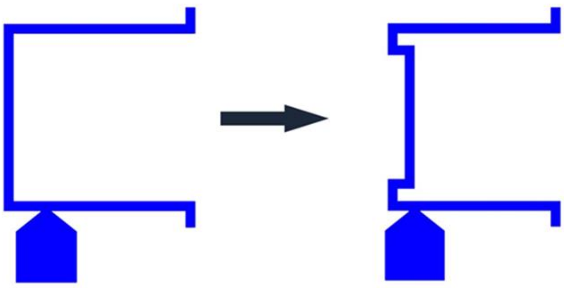

Figure 8: CR Folding for Size Reduction and Enhanced Coupling.

Following the inward folding of the CRs at their midpoints, the central segments are further repositioned towards the interior. Figure 8 illustrates the impact of this adjustment on the filter's performance. As the distance (d) in Figure (9a) is altered, while simultaneously maintaining a consistent CR length through adjustments to (x), the filter's frequency response undergoes changes, as depicted in Figure (9b) and Figure (9c).

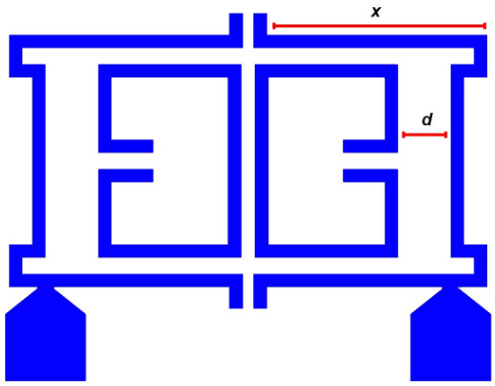

(a)

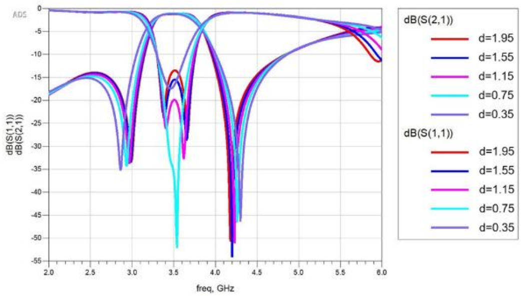

(b)

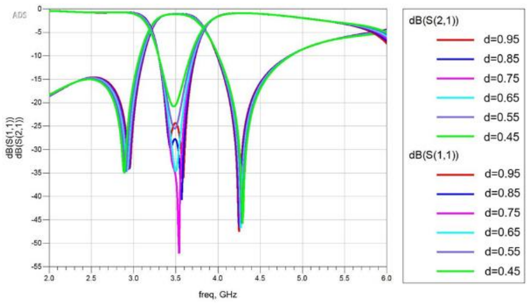

(c)

Figure 9: (a) Further increasing coupling strength between CRs and FRs by decreasing (d); (b) Effect of changing the distance (d) between [0.35 - 1.95 mm] on filter's response; (c) Effect of changing the distance (d) between [0.45 - 0.95 mm] on filter's response.

From the preceding figures, it becomes apparent that a separation of 0.75 mm between the CRs and Folded Resonators (FRs) on both lateral sides achieves the most effective coupling, resulting in the optimal filter performance.

Figure (10a) presents the finalized filter design, showcasing a pair of TZs surrounding the passband, and incorporating the optimized resonator dimensions and inter-resonator spacing. The corresponding frequency response is displayed in Figure (10b).

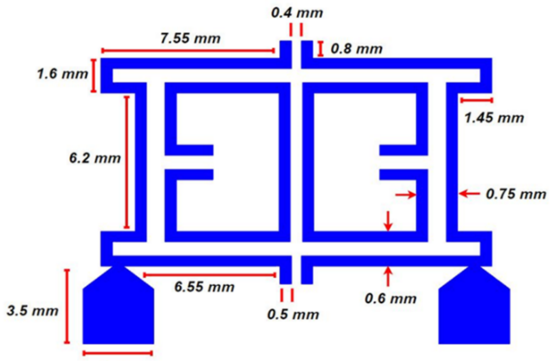

(a)

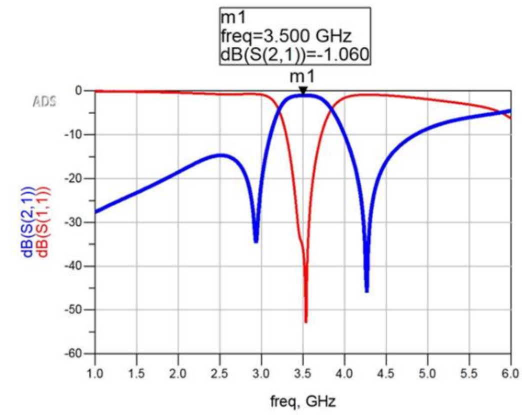

(b)

Figure 10: (a) The proposed BPF's structure with a pair of TZs around the passband (b) Frequency response of the proposed filter.

The filter, as presented in Figure (10), operates at a central frequency of 3.5 GHz, exhibiting a bandwidth of approximately 0.6 GHz. The passband is defined by attenuation starting below 3.2 GHz and above 3.8 GHz. Within this passband, the filter demonstrates a low insertion loss (S21) of approximately -1.1 dB and a desirable return loss (S11) exceeding -40 dB. The occurrence of TZs at the passband's edges (fZ1 and fZ2) contributes to a more abrupt roll-off, effectively obviating the requirement for a higher-order filter configuration.

However, the stopband attenuation, in its current state, is insufficient for peak performance, potentially allowing undesired out-of-band signals, particularly within the sub-6 GHz spectrum, to propagate through. To rectify this, an additional pair of TZs can be integrated around the passband utilizing a zero-degree feed technique.

2.4 Enhanced Stopband Attenuation via Zero-Degree Feed Method

To overcome the limitation of inadequate stopband attenuation, a zero-degree feed methodology is implemented, enabling the introduction of an additional, controllable pair of TZs within the stopband. This technique involves inputting the signal at a diagonal position on symmetrical structures, thereby establishing two signal pathways that exhibit a 0-degree phase difference, as illustrated in Figure 11.

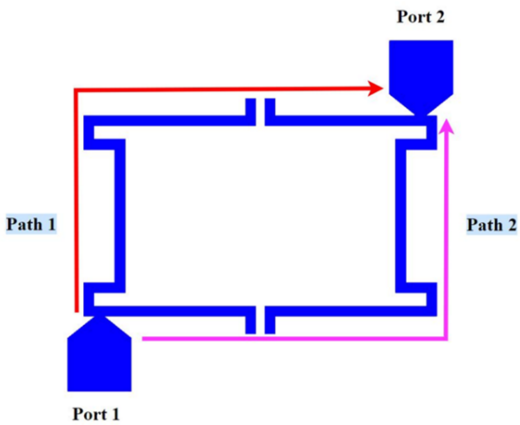

Figure 11: Zero-degree method.

By injecting the signal into the CRs at a designated point, such as point A in Figure (12), the resonator is effectively partitioned into two segments, P1 and P2, characterized by unequal lengths, L1 and L2, respectively, leading to the creation of two transmission zeros. The first TZ occurs at a frequency where its quarter wavelength corresponds to L1, and the second TZ appears at a frequency where its quarter wavelength aligns with L2.

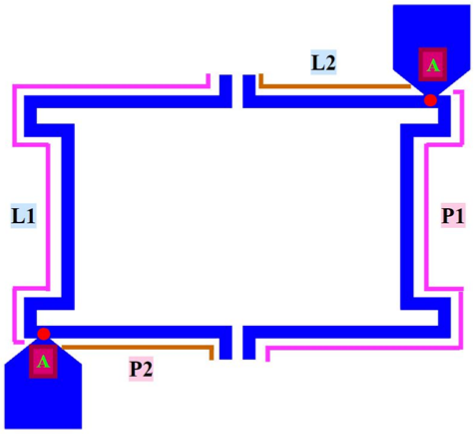

Figure 12: Feeding the CRs at specific points (A).

As shown in the previous figure, section P1 in one CIR corresponds to section P2 in the other. Due to the difference in length, and consequently resonant frequency, when one section (P1 or P2) resonates, the wave does not propagate to the corresponding section or to the FRs, causing signal attenuation at those specific frequencies.

From the preceding figure, section P1 in one CR corresponds to section P2 in the other. Due to the disparity in length, and consequently, resonant frequency, when one section (P1 or P2) resonates, the wave is impeded from propagating to the corresponding section or to the FRs, resulting in signal attenuation at these specific frequencies. Figure (13a) displays the current distribution within the CR at the center frequency of 3.5 GHz, which serves as the foundation for the filter design. The current is distributed across nearly the entire resonator, facilitating a harmonious interaction among the filter components and allowing the desired frequencies to pass. Conversely, Figure (13b) and Figure (13c) illustrate the current distribution at the attenuation frequencies, fz3 = 2.4 GHz and fz4 = 5.23 GHz, respectively. In these instances, the current is confined to sections P1 and P2. The positions of fz3 and fz4 can be adjusted by altering the injection point (A).

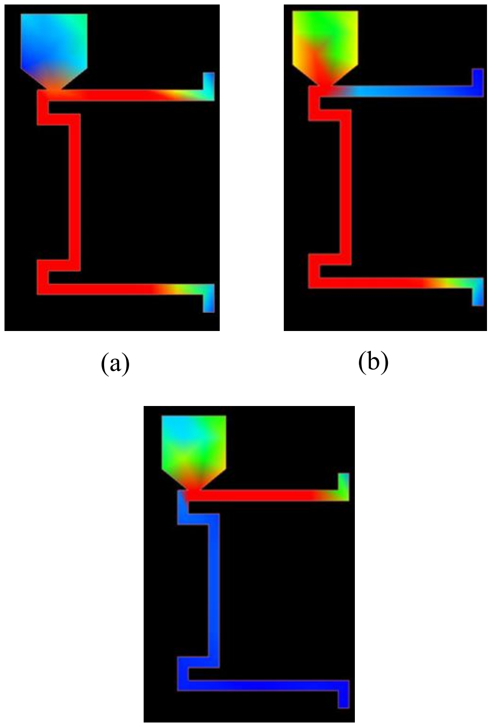

(a) (b)

(c)

Figure 13: Current Distribution: (a) at Center Frequency (3.5 GHz), (b) at fz3 (2.4 GHz), and (c) at fz4 (5.23 GHz).

Figure (14) presents the resulting frequency response after the application of the zero-degree feed technique. A pair of TZs is now observed at fz3 = 2.4 GHz and fz4 = 5.23 GHz in the lower and upper stopbands, respectively. This has significantly enhanced the stopband attenuation.

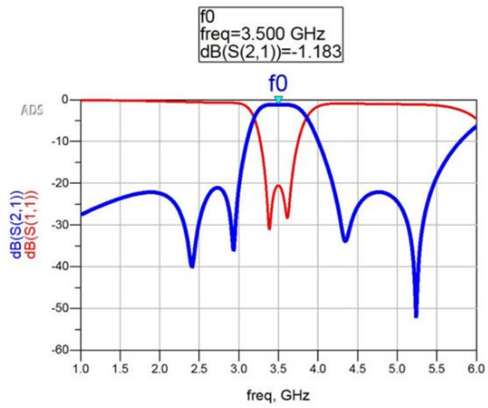

Figure 14: Frequency Response with additional pair of TZs via Zero-Degree Feed.

In the concluding phase, the signal injection points are refined. This process entails precisely adjusting the feed structures by varying the distance (d) on both lateral sides, as illustrated in Figure (15a), while maintaining the integrity of the remaining filter components.

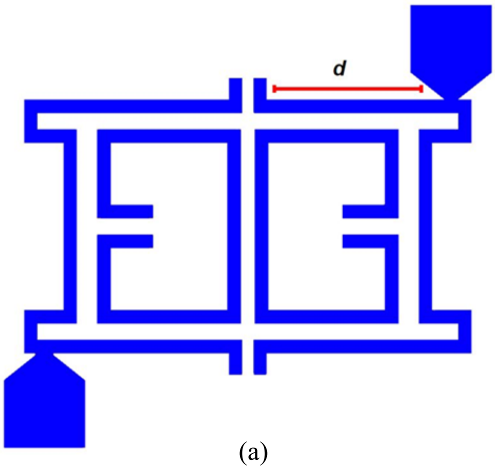

(a)

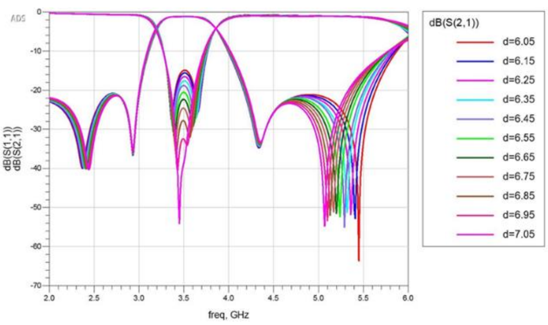

(b)

Figure 15: (a) Adjustment of signal injection points (d); (b) Corresponding frequency response.

Figure (15b) depicts the filter's frequency response across a spectrum of (d) values. As anticipated, alterations to the injection point modify the lengths that determine the generation of TZ3 and TZ4, leading to a corresponding shift in their respective frequencies. Furthermore, adjustments to (d) also optimize the passband response, achieving its ideal configuration when (d = 7.05 mm).

Figure (16) presents the final schematic of the proposed filter, and Table (1) provides the corresponding dimensional specifications, while Figure (17) showcases the finalized filter's frequency response.

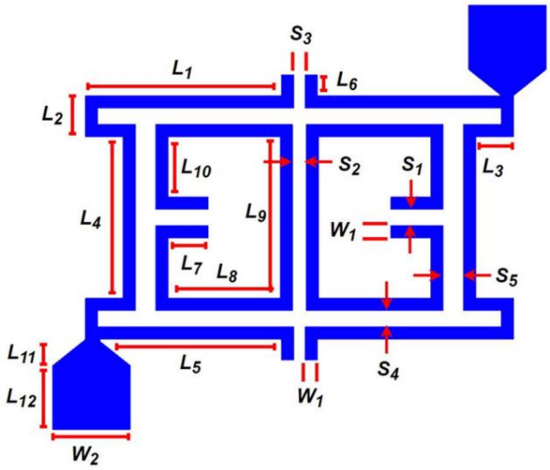

Figure 16: The proposed BPF’ structure with four TZs in the stopband.

Table 1: The proposed BPF’ dimensions all in mm Unit.

L1	**L2**	**L3**	**L4**	**L5**	**L6**
7.55	16	1.45	6.2	7.05	**0.8**
L7	**L8**	**L9**	**L9**	**L10**	**L11**
1.55	4.3	6.2	2.3	1	**2.5**
S1	**S2**	**S3**	**S4**	**S5**	**W1**
0.6	0.5	0.4	0.6	7.5	**0.5**
W2					
3					

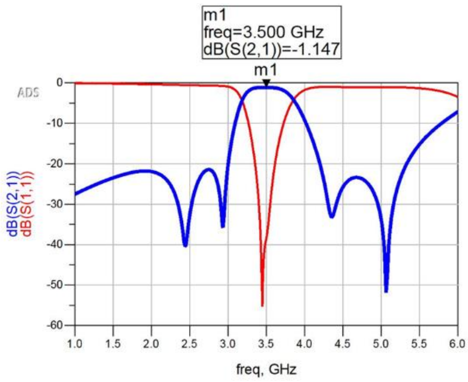

Figure 17: Frequency response of the proposed BPF.

The simulation outcomes reveal a passband cantered at 3.5 GHz, characterized by a transmission coefficient (S21) of -1.147 dB and a -3 dB bandwidth

(BW) of approximately 0.6 GHz. The reflection coefficient (S11) within the passband surpasses -40 dB. Four transmission zeros are generated within the stopband to enhance overall performance.

Moreover, the proposed filter, with dimensions of 0.39 λg × 0.46 λg, demonstrates superior performance compared to other reported studies (Alaydrus et al., 2013, Astuti and Alaydrus, 2013, Chang et al., 2019 , Kadiri et al., 2022, Maulidini et al., 2020), evidenced by its incorporation of four TZs in the stopband, a wider bandwidth, and a more compact form factor. Table (2) provides a comprehensive summary of the key performance metrics for the proposed design. The table also offers a direct comparison between this design and a selection of currently available filters, highlighting its efficiency and distinct advantages.

Table 2: Performance Comparison with Existing Filters.

Ref.	**Center Frequency (GHz)**	**BW (GHz)**	**TZs**	**Size (λg^2)**
Alaydrus et al., 2013	2.45	0.3	2	0.5 × 0.6
Chang et al., 2019	3	0.45	3	0.42 × 0.52
Kadiri et al., 2022	3	0.5	2	0.40 × 0.48
This Work	3.5	0.6	4	0.39 × 0.46

3 Conclusions

This study successfully developed and optimized a compact microstrip bandpass filter at 3.5 GHz, significantly improving its performance through the clever use of folded and coupling resonators. By incorporating both input/output coupling and a zero-degree feed technique, we were able to introduce four transmission zeros, which greatly boosted the filter's ability to block unwanted signals and sharpened its performance curves. Careful fine-tuning of the resonator spacing and feed line positions resulted in a filter with low signal loss and high reflection loss, achieving a useful bandwidth of 0.6 GHz. This new filter, measuring a compact 0.39 λg × 0.46 λg , shows better performance than many existing designs, especially in its small size and excellent ability to suppress signals outside its desired range. This makes it a very promising solution for modern wireless communication systems that need high precision and effective removal of unwanted signals. Its ability to integrate multiple transmission zeros in a small space is a significant step forward, offering a flexible design that can easily fit into tight spaces in future 5G, radar, and satellite systems.

Future Work

Manufacturing the designed filters through printing techniques and rigorously validating the achieved results through experimental testing.

REFERENCES

ALAYDRUS, M., WIDIASTUTI, D. & YULIANTO, T. Designing cross-coupled bandpass filters with transmission zeros in lossy microstrip. 2013 International Conference on Information Technology and Electrical Engineering (ICITEE), 2013. IEEE, 277-280.

ASTUTI, D. W. & ALAYDRUS, M. A bandpass filter based on square open loop resonators at 2.45 GHz. 2013 3rd International Conference on Instrumentation, Communications, Information Technology and Biomedical Engineering (ICICI-BME), 2013. IEEE, 147-151.

CHANG, J., DAI, J. & LI, Y. Design of Microstrip Cross-Coupling Bandpass Filter With High Selectivity and Stopband Suppression Using Internal Coupling SIRs. 2019 International Conference on Microwave and Millimeter Wave Technology (ICMMT), 2019. IEEE, 1-3.

CHRISTIANO, L. J. & FITZGERALD, T. J. 2003. The band pass filter. *International economic review,* 44, 435-465.

COSTANZO, A. & MASOTTI, D. 2017. Energizing 5G: Near- and Far-Field Wireless Energy and Data Trantransfer as an Enabling Technology for the 5G IoT. *IEEE Microwave Magazine,* 18, 125-136.

EZHILARASAN, E. & DINAKARAN, M. A review on mobile technologies: 3G, 4G and 5G. 2017 second international conference on recent trends and challenges in computational models (ICRTCCM), 2017. IEEE, 369-373.
HONG, J.-S. G. & LANCASTER, M. J. 2004. *Microstrip filters for RF/microwave applications*, John Wiley & Sons.
KADIRI, A., TAJMOUATI, A., ZBITOU, J., ZAHRAOUI, I., ERRKIK, A. & LATRACH, M. A New Design of a Miniature Microstrip Bandpass Filter for DCS Applications. E3S Web of Conferences, 2022. EDP Sciences, 01083.
MAULIDINI, R. A., HIDAYAT, M. R. & PRALUDI, T. 2020. Band-pass filter microstrip at 3 GHz frequency using square open-loop resonator for S-band radar applications. *Jurnal Elektronika Dan Telekomunikasi,* 20**,** 53-59.
SHEN, G., CHE, W., FENG, W. & WANG, C. 2019. Realization of multiple transmission zeroes for bandpass filters with simple inline topology. *IEEE Transactions on Circuits and Systems II: Express Briefs,* 67**,** 1029-1033.
SURWASE, M. S., SALUNKHE, M. S., VHATKAR, M. P. & MALI, R. 2017. Design and simulation of compact Hairpin Bandpass filter. *Ijlera. com. Recuperado el,* 16.
THOMPSON, J., GE, X., WU, H.-C., IRMER, R., JIANG, H., FETTWEIS, G. & ALAMOUTI, S. 2014. 5G wireless communication systems: Prospects and challenges [Guest Editorial]. *IEEE communications Magazine,* 52**,** 62-64.
TSAI, C.-M., LEE, S.-Y. & TSAI, C.-C. 2002. Performance of a planar filter using a 0/spl deg/feed structure. *IEEE Transactions on Microwave Theory and Techniques,* 50**,** 2362-2367.

Biography

Thaer A. Sultan: was born in Mosul, earned his B.Sc. in Electronic Engineering from the College of Electronics Engineering, Ninevah University, Iraq, in 2018. He is currently pursuing an M.Sc. at the same institution, with research interests focused on design of microwave bandpass filters for 5G applications.

Dr. Ahmad M. A.Sabaawi: received the B.Sc. and M.Sc. degrees in Electronics and Communication Engineering from Mosul University, Iraq, in 2002 and 2008, respectively, and the Ph.D. degree in Electrical and Electronic Engineering from the School of Engineering, Newcastle University, Newcastle Upon Tyne, U.K. in 2015, where his research focused on designing nano antennas for solar energy collection. He worked as Research Associate at Lancaster University from 2015 to 2017 and as KTP Associate at Newcastle University from 2017 to 2018. Dr. Sabaawi is currently Assistant Prof at the College of Electronics Engineering, Ninevah University, Mosul, Iraq.